PSFC/JA-04-18

Investigation of Performance Limiting Phenomena in a Variable Phase ICRF Antenna in Alcator C-Mod

Wukitch, S.J., Boivin, R.L.,[1] Bonoli, P.T.,[1] Goetz, J.A.,[2] Irby, J.,[1] Hutchinson, I.H.,[1] Lin, Y.,[1] Parisot, A.,[1] Porkolab, M.,[1] Marmar, E.,[1] Schilling, G.,[3] and Wilson, J.R.[3]

June 2004

Plasma Science and Fusion Center
Massachusetts Institute of Technology
Cambridge MA 02139

[1]Current address: GA, San Diego, CA USA
[2]Current address: U. of Wisconsin, Madison, WI USA
[3]Princeton Plasma Physics Laboratory, Princeton, NJ USA

This work was supported by Department of Energy Coop. Agreement DE-FC02-99ER54512.

Submitted for publication in *Plasma Physics and Controlled Fusion.*

Investigation of Performance Limiting Phenomena in a Variable Phase ICRF Antenna in Alcator C-Mod

S.J. Wukitch,[1] R.L. Boivin,[2] P.T. Bonoli,[1] J.A. Goetz,[3] J. Irby,[1] I. Hutchinson,[1] Y. Lin,[1] A. Parisot,[1] M. Porkolab,[1] E. Marmar,[1] G. Schilling,[4] and J.R. Wilson[4]

[1]MIT Plasma Science and Fusion Center, Cambridge, MA 02139 USA
[2]Current address: GA, San Diego, CA USA
[3]Current address: U. of Wisconsin, Madison, WI USA
[4]Princeton Plasma Physics Laboratory, Princeton, NJ USA

Abstract: High power density, phased antenna operation can often be limited by antenna voltage handling and/or impurity and density production. Using a pair of two-strap antennas for comparison, the performance of a four-strap, fast wave antenna is assessed for a variety of configurations and antenna phase in Alcator C-Mod. To obtain robust voltage handling, the antenna was reconfigured to eliminate regions where the RF E-field is parallel to B or reduce the RF E-field to <1.0 MV/m. To limit impurity generation, BN tiles have replaced the original Mo tiles, a BN clad septum was inserted to limit field line connection length, and BN-metal interfaces are shielded from the plasma. With these modifications, the antenna heating efficiency and impurity generation are nearly identical to the 2-strap antennas and independent of antenna phase in L-mode discharges. This antenna has achieved 11 MW/m^2 in both heating and current drive phase in both L-mode and H-mode discharges.

1. Introduction

Ion cyclotron range of frequency (ICRF) power is anticipated to be a primary auxiliary heating source in proposed next step tokamak experiments like ITER and FIRE. Antenna designs are often based upon available experimental experience and theoretical models, but antenna performance appears to be difficult to predict. For example, significant experimental and theoretical effort was invested to develop the A1 (2-strap) ICRF antennas in the Joint European Torus (JET) that coupled 22 MW of ICRF power to the plasma.[1] However, this recipe was less successful when applied to the A2 (4-strap) antennas that coupled 16 MW of ICRF power.[2] In C-Mod, a major concern with the ICRF 2-strap antennas was runaway self-sputtering, particularly from the Faraday screen (FS), due to the high plasma densities and metallic plasma facing components.[3] These antennas have achieved power densities of ~10 MW/m^2 without significant impurity production problems.

In Alcator C-Mod, a compact 4-strap, fast-wave (J) antenna has been developed through an iterative process. The challenge is to reliably deliver 3 MW (4 MW source) through a single horizontal port (63 cm x 20 cm), have a peak operational voltage of 40 kV, heat efficiently and allow for flexible phasing. Limited access dictates a folded strap design and vacuum strip line for the antenna feeds. For better current drive spectrum, the Faraday screen and antenna box are more open than the original two 2-strap (D and E) antennas.[4] The antenna

was first installed in 1999 and had a power limit resulting from explosive impurity generation events (injections) at ~4.7 MW/m^3.[5]

In general, antenna performance can be limited by voltage breakdown, impurity generation and density influx. In this paper, we will concentrate on the arcing and impurity generation. In C-Mod, the time scale of the density increase is of order a confinement time suggesting the density evolution is a result of increased heat flux to plasma facing components; furthermore, the incremental density increase becomes smaller as the machine becomes better conditioned.

Although conceptually a simple phenomenon, the physics of a high voltage arc is complicated by the many effects that can influence the voltage at which arcing occurs. Arcing occurs when a macroscopic current (~μA) flows from a surface. Field emission based on electron tunneling is well described by the Fowler-Nordheim equation[6] and indicates that voltages of order GV/m are required. Even for idealized small electrodes the breakdown voltage is of order 20 MV/m. A number of theories have been proposed to explain this discrepancy including enhanced field emission due to local surface protrusions, gas adsorption, and macro-particle exchange.[7,8] Additional complications in tokamak plasmas include ionizing radiation and energetic neutrals during plasma operation, relatively high neutral pressure (~0.1-1 mTorr in C-Mod), line transients from loading variations, and multipactoring. In C-Mod, electrical breakdown was inferred to be as low as E~1.5 MV/m where the RF E-field is parallel to the tokamak B-field (E||B) and the antennas have achieved at E~3.5 MV/m for E⊥B during plasma operation (maximum limit may be higher). Early breakdown studies for ICRF antennas suggested that E-fields of ~0.9 MV/m and 5 MV/m could be supported where E||B and E⊥B, respectively.[9] Other experiments have observed similar degradation of the antenna voltage performance in the presence of plasma.[10] In the J antenna, the voltage limitation was identified to be a result of E||B.

From the first ICRF experiments on tokamaks, increased impurity and density production has been associated with RF operation.[11] Faraday screens and protection limiters have become standard antenna components. Faraday screens were empirically found to protect the antenna from direct plasma interactions and improve voltage handling and heating efficiency. However in JET, the FS was identified as the primary source of impurities during ICRF operation[12] and a number of mechanisms have been proposed.[3,13,14,15] One recipe for FS design has been to minimize the RF sheaths, minimize plasma density at the FS, and use a material with a low self-sputtering coefficient. These considerations suggest that aligning the

FS rods to the magnetic field line pitch and a large number of FS rods (short connection lengths) are desirable features. Protection limiters are important to limit the density at the FS and low Z metals like Be have been demonstrated to reduce the impurity influx associated with ICRF operation.[16] Other strategies have been implemented including removing the Faraday screen[17,18,19,20] and minimizing the path length between rod elements coated with low sputtering material. Impurity and density production has been observed to be minimized for heating (0-π) phasing for 2-strap antennas.[21] For other phases, the impurity production increases for current drive phasing and is maximum for the so-called mono-pole (0-0) phasing.[22,23] Given the complex nature and lack of a clear theoretical prediction for antenna performance, an empirical approach was adopted to overcome performance limitations due to arcing and impurity generation in the J antenna. In the following, a brief description of the C-Mod antennas and their key design features is presented. Followed by a comparison of the antenna performance where the D and E antennas are used as a benchmark as a result of their proven operational success.

2. Antenna Description

The C-Mod ICRF antennas are required to withstand high heat loads, large disruption forces, and high RF voltages in presence of 0.1-1 mTorr neutral pressures. The D and E-antennas have delivered 3.5 MW (~10 MW/m^2) through two horizontal ports and have a fixed dipole phase.[4] The J-antenna has achieved 3 MW (11 MW/m^2) operation through a single horizontal port and can be phased. All the antennas originally used TiCN coated molybdenum (Mo) protection tiles; however, the Mo core content was found to scale proportional to the RF power.[24] The primary impurity source was identified as the antenna limiters rather than the FS (TiCN coated over Cu-plated Inconel 625 rods). Although the antenna limiter Mo sources are lower in magnitude than the inner wall or divertor, the impurity screening at the outboard mid-plane is significantly poorer than either the inner wall or the divertor. As discussed earlier, impurity production can result from the increased sputtering resulting from rectified RF sheaths on metallic surfaces. To eliminate the Mo source and prevent the sheaths from developing particularly in current drive phase, the Mo tiles have been replaced with insulating BN, AXO5 grade from Saint-Gobain Advanced Ceramics.

The D and E antennas (the D antenna is shown in Figure 1) have end-fed, center grounded current straps and 30 Ω strip line vacuum transmission lines (VTL) where the RF E-field is

perpendicular to tokamak B-field. The Faraday screen is aligned with the nominal B-field pitch (~10°) and is ~27% optically transparent. The screen elements are 0.95 cm diameter Cu-plated (4-8 μm) Inconel 625 rods welded to the antenna box at both ends. The Faraday rods are coated with TiCN on D antenna and B_4C on E antenna. Due to the large disruption forces generated by ~1 T/msec quenches and large toroidal B-field, the rod's radial arm is short, ~3.5 cm, and is welded into a solid 1.25 cm Inconel 625 plate. The mid-plane major radius (R) location of the antenna limiters are at R=91.3 cm, ~0.8 cm behind the main plasma limiters. The Faraday screen is at R=91.7 cm and the straps are at R=93.5 cm. The straps are separated by 25.75 cm on center and the straps are 10 cm wide. For 0-π phasing, these antennas have a toroidal mode number (n_ϕ) spectrum peaked at ±10 or $k_{||} \approx \pm 11$ m^{-1} at the antenna straps. In this paper, we present results from D and E antennas in two configurations: (1) antenna with Mo tiles replaced by BN, and (2) antenna modified to eliminate plasma facing BN-metal interfaces (current version). When referencing these different versions, they will be referred to as D and E antennas v.1 and v.2, respectively.

Figure 1: D antenna with BN (white) tiles installed.

The J antenna, shown in Figure 2, is a folded strap (see Figure 3 for comparison of D and J-port antenna strap) with a single tap and the VTL is a combination of 4" coaxial transmission line and parallel plate transmission line. The Faraday screen is 50% optically transparent and parallel to the toroidal B-field. The rods have a "W" shape with the center leg bolted to antenna ground and the other two ends have a 0.1 Ω impedance to ground to minimize disruption induced currents. This 0.1 Ω connection consists of a nichrome wire wound around an insulated bobbin covered by ceramic except for two tabs that make contact with the rod and antenna box. To eliminate arcing between this connection and the current strap, a stainless steel shield was installed to interrupt the arc path and shield the ceramic from plasma. The rod's radial arm is ~10 cm and the resulting antenna box is quite open. At the

Figure 2: J antenna installed in C-Mod with antenna septum. (The white tiles are BN.)

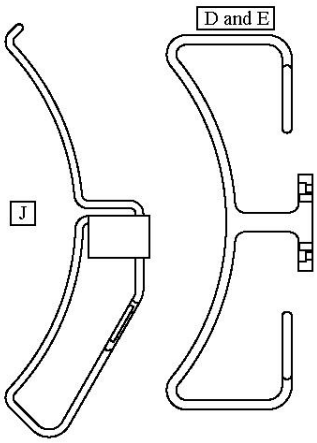

Figure 3: J antenna folded strap design compared to center grounded configuration of D and E antennas.

mid-plane major radius, the antenna limiters are R=91.2 cm, ~0.7 cm behind the main plasma limiters, and the septum is at R=91.6 cm (~2 mm in front of FS). The septum is behind the side tiles in real space to account for the toroidal field ripple between the toroidal field magnets. The Faraday screen face is at R=91.8 cm and the straps are at R=93.6 cm. The current straps are separated by 18.6 cm on center and the straps are 8 cm wide. With straps #1-#3 and #2-#4 connected in (0-0) phasing, the antenna can be run with so-called dipole phasing (0-π-0-π and n_ϕ=±13) or monopole phasing (0-0-0-0 and n_ϕ=±4). With straps #1-#3 and #2-#4 connected with (0-π) phasing, the antenna phase can be either heating phase (0-π-π-0 and n_ϕ=±10) or ±90° phasing (0-±π/2-π-±3π/2 and n_ϕ=±7) where the +90° and -90° phasing launches waves directed co- and counter to the tokamak plasma current, respectively.

In this paper, the results from several antenna versions are presented. For J.v.1, the BN protection tiles were mounted in such a fashion as to leave a BN-metal interface exposed to the plasma. The VTL had sections where the RF E-field was parallel to the tokamak B-field and no septum was installed at this time. The J.v.2 antenna had protection tiles that completely covered the front Mo tiles with recessed fasteners facing the plasma and had a septum installed between straps #2 and #3. The VTL is configured to have the RF E-field oriented perpendicular to the tokamak B-field. The J.v.3 has the BN-metal interfaces completely shielded from the plasma and the antenna strap is modified to reduce the RF E-field where E||B to below 1.0 MV/m in the antenna.

3. Experiment Description

Alcator C-Mod is a compact, high field diverted tokamak.[25] The discharges to be discussed in the following were performed at a toroidal magnetic field (B_T) of 5.2 T and plasma current (I_P) of 0.8 MA. The typical target discharge central density (n_{e0}) was 1.5 x 10^{20} m^{-3} and an electron temperature (T_e) of 1.25 keV. An overview of the antenna location in C-Mod is shown in Figure 4. The absorption scenario used in the following experiments is H minority in D majority and unless otherwise noted the operating frequency of the D, E and J antennas is 80.5 MHz, 80 MHz, and 78 MHz, respectively. This places the H cyclotron resonance 1 cm to the high field side of the magnetic axis for D and E antennas and 1 cm to the low field side of the magnetic axis for the J antenna. The H to D ratio is typically 5-8% as determined by the ratio of H_α to D_α in the plasma edge.[26]

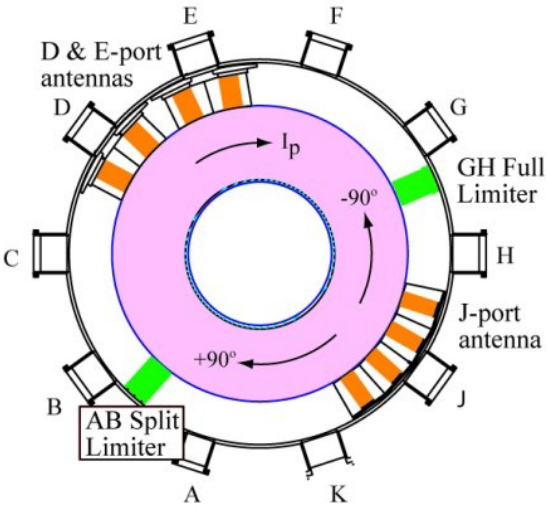

Figure 4: Location of D, E, and J antennas and plasma limiters in C-Mod. Note for the J antenna +90° phasing launches waves in the co-current direction and -90° phasing injects waves in the ctr-current direction.

The primary plasma diagnostics are as follows. The stored plasma energy (W_{Plasma}) is derived from EFIT[27] and T_e is measured via electron cyclotron emission using the 9 channel grating polychromator.[28] The n_{e0} is measured using Thomson scattering[29] and the line averaged density ($\bar{n}_e$) is derived from central chord of the interferometer divided by its plasma chord length determined from EFIT. The neutron rate (R_{neut}) is measured by He^3 detector array[30] and the radiated power is measured by both a diode[31] and calibrated foil array.[32] The effective plasma charge (Z_{eff}) is determined from the measured bremsstrahlung[33] and the edge D_α emission is measured using a diode array.[34]

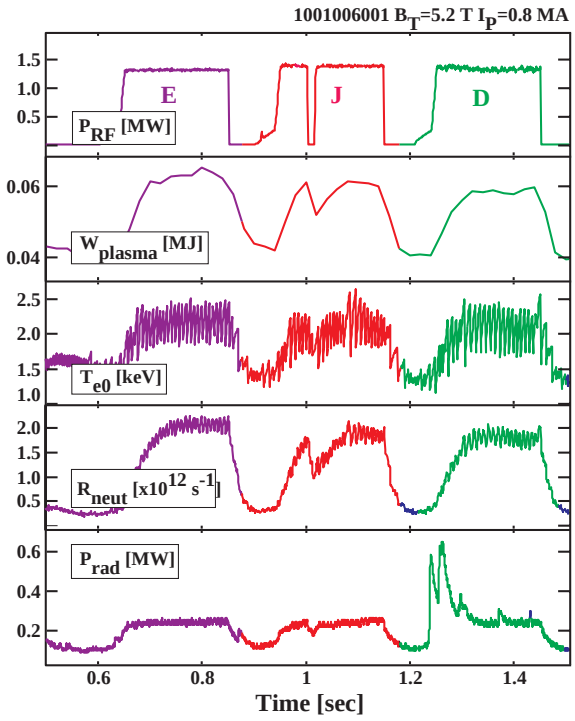

Figure 5: Comparison of D, E, and J antennas shows identical plasma response in L-mode discharges for heating phase.

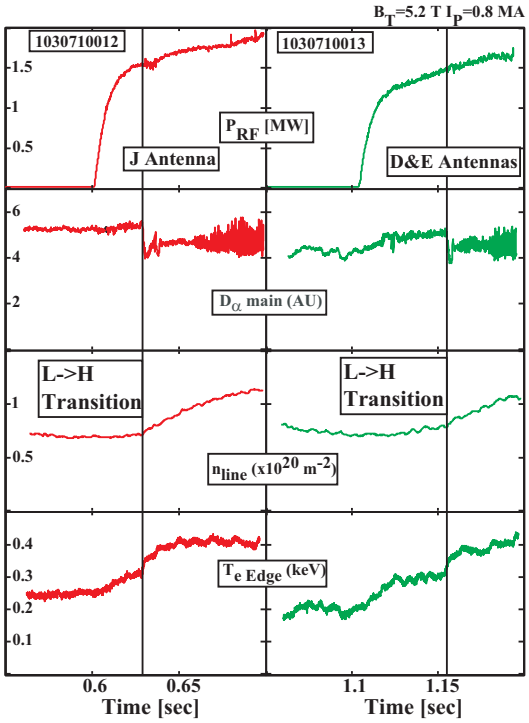

Figure 6: The H-mode power threshold is the similar for the antennas suggesting the heating efficiency is similar.

4. Antenna Performance

4.1 J-port v.1 comparison with D and E-port v.1

The J.v.1 performance was compared to the D and E.v.1 in a series of L-mode discharges using D(H) minority heating. The plasma response to 1.4 MW from E, J, and D antennas is shown in Figure 5. The increase in W_{Plasma}, central T_e, and R_{neut} is similar for all three antennas. The $\bar{n}_e$ remains constant and the P_{rad} has a small increase for all three antennas (ignoring the injection which occurs before D antenna is at power). At this power level, the J antenna has a similar response, indicating similar performance, as the D and E antennas. To investigate heating effectiveness, the power required to initiate a transition to H-mode was measured for each antenna within a single discharge. As shown in Figure 6, the antennas have nearly identical H-mode power thresholds indicating similar heating effectiveness.

The maximum voltage achieved by J.v.1 was limited to 17 kV at 78 MHz while D and E v.1 operated routinely to 35-40 kV. A post-campaign inspection found significant arc damage in regions where E||B. The E-field (V/spacing) limit was estimated to be ~1.5 MV/m for E||B. The voltage limit was significantly lower than the 40 kV achieved in vacuum conditioning of J.v.1 and the 40 kV achieved on D and E.v.1 in plasma operation. In addition to limited

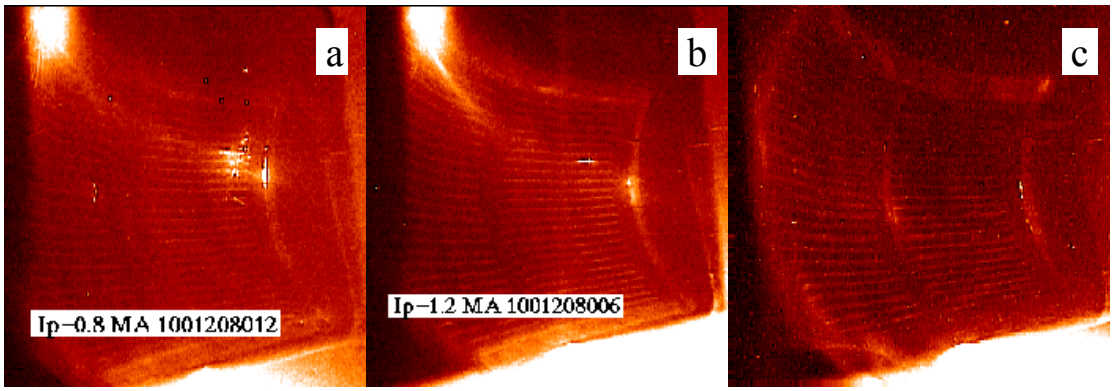

Figure 7: Visible camera views of J antenna during three discharges. Figure (a) and (b) are 0.8 MA and 1.2 MA discharges, respectively, with 2.25 MW injected power. Figure (c) is a 0.8 MA discharge with similar plasma parameters as (a) and 2 MW injected power. Figures (a) and (b) show the strong edge interaction observed before a BN septum was installed and show that the interaction followed a field line. Figure (c) shows the improvement with the addition of the BN septum.

voltage handling characteristics, a strong edge interaction at ~7 MW/m^2 was observed using a visible camera shown in . The interaction was found to scale with plasma q and appeared on the longest field line connection.

4.2 J-port v.2 performance

With reoriented VTL and a BN septum between straps #2 and #3, the antenna maximum voltage increased to 25 kV at 78 MHz and 30 kV was achieved at 70 MHz. This frequency dependence suggested that the arcing was located in the antenna strap itself (see Discussion). The maximum voltage on the antenna decreased as the driving frequency decreased (antenna strap becomes shorter in comparison to the wavelength.) Using an electromagnetic solver, the peak electric field was found to be directed along the B-field and locally obtained ~1.5 MV/m. The plasma edge interaction was reduced as shown Figure 7c. At power densities approaching 9 MW/m^2, impurity injections were again observed. A post-campaign inspection found melt damage on the tile fasteners facing the plasma.

4.3 J-port v.3 performance

With the antenna strap modification and new BN tile fastening technique, power densities of 11 MW/m^2 and maximum voltages of 35 kV have been achieved without significant impurity production in dipole phasing.

To test the antenna performance with other antenna phases, a series of inner wall limited, L-mode discharges were performed where J antenna (v.3 unless otherwise specified) was

phased at heating (0,π,π,0) or ±90° (0, ±π/2, ±π, ±3π/2) and compared to the combined power of D and E antennas (v.2). With J in heating phase, the plasma response to the applied RF power is similar for both pulses. As shown in Figure 8, the W_{Plasma}, central T_e, and D_α are similar (<10% difference) for the two RF pulses. The $\bar{n}_e$, and the P_{rad} have a small and similar increase as well. This indicates the heating effectiveness and density and impurity production are similar to those of the combined D and E antennas for this antenna phase. Identical discharges were performed comparing +90° and -90° phasing and the plasma response is shown in Figure 9. Aside from the sawtooth period, which is longer for +90° than for -90°, the plasma response is similar (<10% variation) and independent of the antenna phasing.

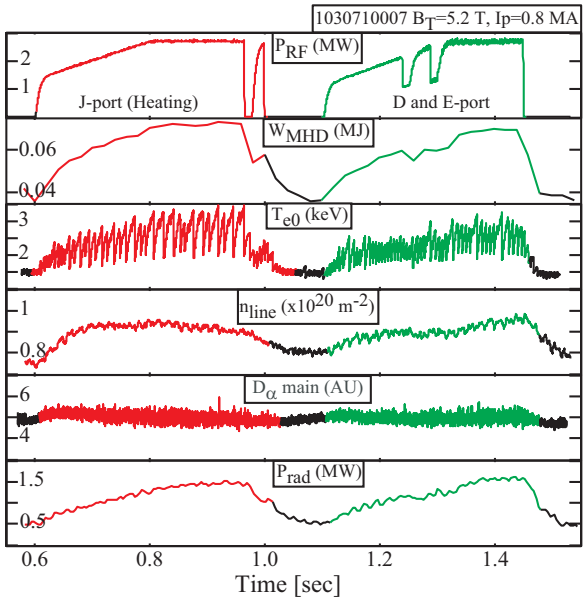

Figure 8: In L-mode, the antenna performance appears to be nearly identical for J in heating phase compared to D and E antennas.

5. Discussion

The reduced breakdown voltage appears to be related to having E||B. Arc damage has been observed in the strip line power feeds in J.v.1 and the antenna strap itself in J.v.2. In J.v.1, the voltage reaches a maximum value for 78 MHz in the VTL where the RF E-field is parallel to the tokamak B-field. The maximum voltage during plasma operation was 17 kV corresponding to ~1.5 MV/m (maximum voltage divided by the strip line spacing). Upon orientating VTL so that the RF E⊥B, the antenna maximum voltage increased to 25 kV at 78 MHz. Further evidence of this empirical limit comes from the frequency dependence of the maximum voltage in J.v.2. At 78 MHz, the maximum voltage was 25 kV and increased to 30 kV at 70 MHz. This suggested the arcing location at the grounding bridge in the antenna strap itself, and a post campaign inspection found the arc damage at this location. Furthermore, the arc damage was located where the geometry would result in local enhancement of the E-field and where the E||B. Modeling of the antenna strap indicated the peak electric field was directed along the field line. The strap configuration was modified to increase the spacing and the electrode was shaped to reduce peaked fields. The peak fields

were reduced by 40% and directed across the B-field. The J.v.3 achieved 35 kV during plasma operation. From this work, we limit the equivalent parallel plate E-field parallel to the B-field to <1.0 MV/m but one needs to examine more closely situations where geometry may enhance the local E-field along the B-field.

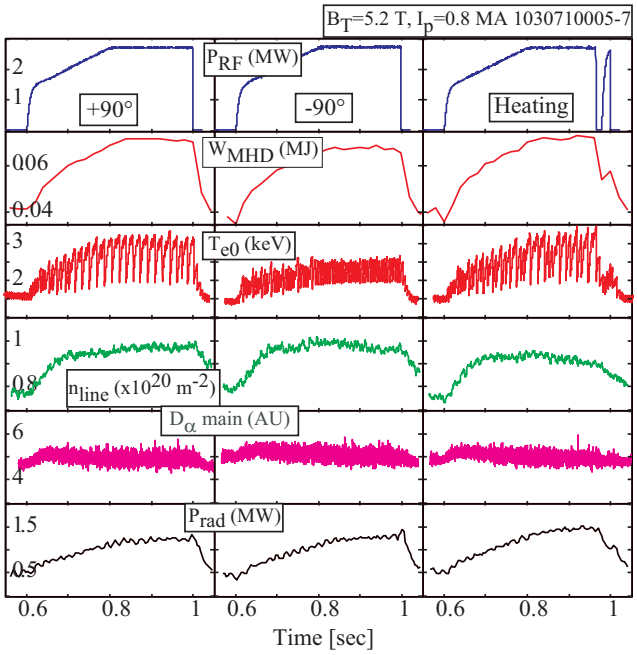

Figure 9: Plasma response is similar for the various J antenna phases suggesting the performance is independent of antenna phase.

The decreased breakdown voltage with E||B has been noted on Tore Supra and JET. In fact, arcing parallel to the B-field at a conical ceramic support limited the performance of the JET A2 antenna.[35] In the C-Mod J antenna, the peak E-fields parallel to B-field clearly limited the antenna performance. Furthermore, the degraded voltage handling of antennas in plasmas has been attributed to ionizing radiation, the presence of energetic neutrals, or line transients due to changes in coupling. The observed E||B limit appears independent of ionizing radiation and energetic neutrals. The limiting region (E||B) was shielded from the direct plasma, energetic neutrals, soft x-ray, and ultraviolet radiation in J.v.1 VTL and exposed in J.v.2 current strap. Line transients also appear to have limited influence on the breakdown voltage. The same limit was observed over a wide variety of plasma discharges (H and L-mode) including H->L transitions and no further degradation of performance was observed.

The reason for the degradation in breakdown voltage with E||B can only be postulated. The estimated local E-fields are < 5 MV/m and field emission becomes important near 20 MV/m. The electron mean free path is much greater than the electrode spacing indicating this combination of E-field, geometry and gas pressure is away from the minimum in the Paschen curve and multipactoring does not appear to be a candidate either. According to Craggs and Meeks,[36] ions govern the breakdown process since the electrons are swept from the spacing between the electrodes during a half cycle. Ion bombardment of the electrode and the

corresponding secondary electron emission results in a streamer formation. The parallel B-field may enhance this process by preventing ion diffusion.

Impurity injections have been empirically determined to be from the exposed BN-metal interfaces in J.v.2. As mentioned above, BN tiles were installed to reduce the metal impurities from the antennas. At BN-metal interfaces exposed to the plasma, injections were observed via visible cameras, and melt damage was found at these interfaces. Field enhancement in the gap between the BN tile and metal surface has been postulated as the cause of the injections.

According to D'ippolito et al.,[3] impurities generated by the screen are a result of sheaths developed along a field line intersecting two Faraday screen elements. If the Faraday screen is well aligned with total B-field, no sheaths would form between FS elements. If the FS elements are misaligned with B-field slightly, this connection length could be long resulting in a high rectified field. Keeping the connection length short can also prevent high rectified fields and this appears to work here.

A somewhat surprising result is the phase independent antenna performance in L-mode. This insensitivity to antenna phase is contrary to the impurity dependence on phase observed in JET[22] and TFTR[23] but consistent with results from unshielded antenna operation in TEXTOR.[37] This result while encouraging is difficult to quantify. The L-mode discharges have relatively low impurity confinement and differences between phases may require a more sensitive experimental approach although this has not been the case for past experiments. One could imagine using H-mode discharges with higher plasma current (leading to higher impurity confinement times) to probe for subtle differences in the impurity production rate and monitors of FS materials like Ti and Ni. There could also be physics explanations to the antenna phase independent performance. The BN side tiles and BN septum prevent large rectified fields from developing along field lines that would result in increased sputtering. The FS, however, has field line connections but either the rectified fields are insufficient to cause significant sputtering or the TiCN coating reduces sputtering. Another reason could be low plasma density at the screen from the combined septum and side limiters. In C-Mod, the density scrape-off length is ~3 mm placing the FS at least one e-folding length behind the side tiles and septum.

Although the J antenna appears to have good power handling and impurity production characteristics in discharges presented here, there are conditions under which the antenna performance degrades or improves. For example, high neutral pressure (>0.3 mTorr) discharges have degraded voltage handling for the J antenna compared to D and E antennas. Another example of degraded voltage handling is low (<0.4 MA) plasma current operation. In He discharges, the voltage handling appears to be improved compared to deuterium discharges. These examples of degraded or improved voltage handling may allow further insight into the physics of ICRF antenna voltage handling and will be addressed in future work.

6. Conclusion

Four-strap variable phase ICRF antenna has been developed and provides performance comparable to the D and E antennas with a power density of 11 MW/m^2 and heating effectiveness and impurity generation independent of antenna phase. The antenna configuration was modified to maintain the RF E-field to be <1.0 MV/m in regions where E||B. Furthermore, impurity generation and injections have been eliminated using BN protection tiles where the BN-metal interface is sufficiently shielded from the plasma.

Acknowledgements

The authors would like to thank W. Beck, P. Koert, and R. Viera for their insight and engineering expertise during the many modifications to the antenna. We would also like to thank the Alcator C-Mod team help and patience in obtaining these results. This work is supported by Department of Energy Coop. Agreement DE-FC02-99ER54512.

References

[1] A. Kaye, *Fusion Eng. Des.* **24**, 1 (1994).
[2] A. Kaye, 16th Symp. Fusion Engineering (IEEE, Piscataway, NJ, 1995), p. 736.
[3] D.A. D'Ippolito et al., *Plasma Phys Control Fusion* **33**, 607 (1991).
[4] Y. Takase et al., 14th Symp. Fusion Engineering ((Piscataway, NJ):IEEE, San Diego, 1992), p. 118.
[5] G. Schilling et al., 13th Topical Conf. Radio Frequency Power in Plasmas, vol. 485 ((Melville, NY): AIP, Annapolis, 1999), p. 429.
[6] R.H. Fowler and L. Nordheim, *Proc. Roy. Soc. London* **A119**, 173 (1928).
[7] H.A. Schwettman, J.P. Turneaure, and R.F. Waites, *J. Applied Physics* **45**, 914 (1974).
[8] R.V. Latham, *IEEE Trans. Electrical Insulation* **EI-19**, 194 (1983).
[9] F.W. Perkins and R.F. Kluge, *IEEE Trans. Plasma Sci.* **PS-12**, 161 (1984).
[10] H. Kimura, T. Imai, and T. Yamamoto, *Nucl. Fusion* **35**, 619 (1997).

[11] P.L. Colestock et al., *J. Vac. Sci. Technology A* **3**, 1211 (1984).
[12] M. Bures et al., *Plasma Phys. Control. Fusion* **33**, 937 (1991).
[13] F.W. Perkins, *Nucl. Fusion* **29**, 583 (1989).
[14] S. Riyopoulos, *Nucl. Fusion* **35**, 261 (1995).
[15] D.A. D'Ippolito et al., *Nucl. Fusion* **38**, 1543 (1998).
[16] M. Bures et al., *Nucl. Fusion* **32**, 1139 (1992).
[17] R. Van Nieuwenhove et al., *Nucl. Fusion* **31**, 1770 (1991).
[18] G. Van Oost et al., *Controlled Fusion and Plasma Physics*, 20th European Phyiscal Society Conf., vol. 17C (Lisbon, 1993), Vol. 17C, p. 671.
[19] R. Majeski et al., Radio Frequency Power in Plasmas, vol. 244(AIP, 1992), p. 322.
[20] J. Sorensen et al., *Nucl. Fusion* **33**, 915 (1993).
[21] M. Bures et al., *Plasma Phys. Control. Fusion* **30**, 1833 (1988).
[22] M. Bures et al., *Plasma Phys. Control. Fusion* **30**, 149 (1988).
[23] J.E. Stevens et al., *Plasma Phys Control. Fusion* **32**, 189 (1990).
[24] B. Lipschultz et al., *Nucl. Fusion* **41**, 585 (2001).
[25] I.H. Hutchinson et al., *Physics of Plasmas* **1**, 1511 (1994).
[26] T.E. Tutt, *H-Alpha/D-Alpha Spectroscopy on Alcator C-Mod*, PSFC/RR-99-11(MIT Plasma Science and Fusion Center, Cambridge MA, 1999).
[27] L. L. Lao, H. St. John, R. D. Stambaugh, A. G. Kellman, and W. Pfeiffer, *Nucl Fusion* **25**, 1611 (1985).
[28] A. Hubbard et al., *Physics of Plasmas* **5**, 1744 (1998).
[29] J.W. Hughes et al., *Rev. Sci. Instrum.* **74**, 1667 (2003).
[30] C. L. Fiore and R. L. Boivin, *Rev. Sci. Instrum.* **66**, 945 (1995).
[31] R.L. Boivin et al., *Rev. Sci. Instrum.* **70**, 260 (1999).
[32] J. A. Goetz et al., *J. Nucl. Mater.* **220**, 971 (1995).
[33] E.S. Marmar et al., *Rev. Sci. Instrum.* **72**, 940 (2001).
[34] J.A. Goetz et al., *Phys. Plasmas* **3**, 1908 (1996).
[35] A S Kaye, *Plasma Phys. Control. Fusion* **35** (A), 71 (1993).
[36] Craggs, in *Electrical Breakdown of Gases*, edited by Meek and Craggs (John Wiley & Sons, New York, 1978), pp. 689-716.
[37] R. Van Nieuwenhove, *Nucl. Fusion* **32**, 1913 (1992).